AGU PUBLICATIONS

JGR

Journal of Geophysical Research: Oceans

RESEARCH ARTICLE

10.1002/2015JC010754

Key Points:
- Tides and seasonal river discharge influence flow and sediment dynamics
- River exports sediment to shelf during high flow and imports during low flow
- Physical mechanisms of sediment transport differ between high and low flow

Correspondence to:
D. J. Nowacki,
nowacki@uw.edu;
dnowacki@usgs.gov

Citation:
Nowacki, D. J., A. S. Ogston, C. A. Nittrouer, A. T. Fricke, and D. T. Van Pham (2015), Sediment dynamics in the lower Mekong River: Transition from tidal river to estuary, *J. Geophys. Res. Oceans*, *120*, 6363–6383, doi:10.1002/2015JC010754.

Received 30 JAN 2015
Accepted 24 AUG 2015
Accepted article online 26 AUG 2015
Published online 23 SEP 2015
Corrected 7 OCT 2015

This article was corrected on 7 OCT 2015. See the end of the full text for details.

Sediment dynamics in the lower Mekong River: Transition from tidal river to estuary

Daniel J. Nowacki[1,2], Andrea S. Ogston[2], Charles A. Nittrouer[2], Aaron T. Fricke[2], and Van Pham Dang Tri[3]

[1]Now at U.S. Geological Survey, Woods Hole, Massachusetts, USA, [2]School of Oceanography, University of Washington, Seattle, Washington, USA, [3]Department of Environment and Natural Resources Management, Can Tho University, Can Tho, Vietnam

Abstract A better understanding of flow and sediment dynamics in the lowermost portions of large-tropical rivers is essential to constraining estimates of worldwide sediment delivery to the ocean. Flow velocity, salinity, and suspended-sediment concentration were measured for 25 h at three cross sections in the tidal Song Hau distributary of the Mekong River, Vietnam. Two campaigns took place during comparatively high-seasonal and low-seasonal discharge, and estuarine conditions varied dramatically between them. The system transitioned from a tidal river with ephemeral presence of a salt wedge during high flow to a partially mixed estuary during low flow. The changing freshwater input, sediment sources, and estuarine characteristics resulted in seaward sediment export during high flow and landward import during low flow. The Dinh An channel of the Song Hau distributary exported sediment to the coast at a rate of about 1 t s^{-1} during high flow and imported sediment in a spatially varying manner at approximately 0.3 t s^{-1} during low flow. Scaling these values results in a yearly Mekong sediment discharge estimate about 65% smaller than a generally accepted estimate of 110 Mt yr^{-1}, although the limited temporal and spatial nature of this study implies a relatively high degree of uncertainty for the new estimate. Fluvial advection of sediment was primarily responsible for the high-flow sediment export. Exchange-flow and tidal processes, including local resuspension, were principally responsible for the low-flow import. The resulting bed-sediment grain size was coarser and more variable during high flow and finer during low, and the residual flow patterns support the maintenance of mid-channel islands.

1. Introduction

Rivers are the largest suppliers of sediment to the global ocean and deliver 13 Gt yr^{-1} today [*Syvitski and Kettner*, 2011]. This value is the worldwide summation of sediment discharge values determined at the lowermost river gauging stations, which are almost always upstream of tides. The ungauged regions, which include tidal rivers (i.e., freshwater but tidally varying) and their floodplains, deltas, estuaries, and nearshore zones, likely trap great amounts of sediment [*Milliman and Farnsworth*, 2011]. In large rivers, these areas may sequester about one third of the reported sediment discharge (Amazon [*Nittrouer et al.*, 1995; *Mertes et al.*, 1996; *Dunne et al.*, 1998]; Ganges-Brahmaputra [*Goodbred and Kuehl*, 1998]; Changjiang [*Milliman et al.*, 1985]). These ungauged environments are extensive, and a considerable portion of sediment transported in them does not reach the continental shelf. The importance of knowing accurate global riverine sediment discharge rates to the ocean motivates this investigation into hydrodynamic and sedimentary processes.

There are many methods for predicting the character of tidal rivers and estuaries. Nearly all of these approaches base their predictions on the competition between river flow, which provides stratification, and tidal flow, which provides mixing [*Dyer*, 1997]. Variability in river flow can come in the form of flood events, seasonal discharge changes, and long-term climatic shifts; tidal variability is primarily driven by daily and spring-neap cycles. This paper focuses on the changes induced by different seasonal discharge levels. Estuarine regime shifts driven by seasonal river discharge variability have long been observed [e.g., *Hansen and Rattray*, 1966] in estuaries and deltas of all sizes. For example, the Columbia [*Hughes and Rattray*, 1980], San Francisco Bay [*Walters et al.*, 1985], Tamar [*Bale et al.*, 1985], and Merrimack [*Ralston et al.*, 2010] estuaries transition from highly stratified to moderately stratified conditions depending on seasonal river discharge.

The same variables that affect stratification also influence the suspended-sediment dynamics of the tidal river and estuary. Seasonal shifts in sediment-transport patterns have been observed in the Chesapeake Bay [*Schubel*, 1968], Fraser [*Milliman*, 1980], Columbia [*Gelfenbaum*, 1983], Amazon [*Kineke and Sternberg*, 1995], and Hudson [*Woodruff et al*., 2001] estuaries, and these shifts can also modify the character of the seabed [*Kuehl et al*., 1996]. The nature of this variability determines potential sediment storage and release along the tidal river and, in turn, the magnitude and timing of sediment discharge to the coastal ocean.

One technique used to explore the impacts of varying fluvial and tidal influence is decomposition of the tidally averaged (or residual) flux of salt or sediment into several terms. Flux decomposition is used to attribute physical processes (e.g., river advection, exchange flow, tidal pumping) to the observed characteristics of a tidal system. Decomposition is most often applied to salt transport [e.g., *Fischer*, 1972, 1976; *Dyer*, 1974; *Uncles and Jordan*, 1979; *Hughes and Rattray*, 1980; *Dronkers and van de Kreeke*, 1986], and the process is also used with sediment flux [*Dyer*, 1978; *Uncles et al*., 1985a,b; *Su and Wang*, 1986]. Despite frequent usage of the technique, the specific implementation often differs among investigations and publications, and the number of terms retained in the decomposition can range from two to eight or more.

We made observations on a distributary channel of the lower Mekong River delta during high-discharge and low-discharge periods to characterize its hydrodynamics and sediment dynamics. In addition to confirming previously observed seasonal changes of the tidal river and estuarine region of the lower Mekong [*Wolanski et al*., 1996, 1998], we sought to understand better the tidal-scale dynamics and spatial variability of this system, and how river flow modifies these characteristics. Our objectives in this work are: to quantify the changes in hydrodynamics and sediment transport on multiple temporal and spatial scales; to decompose the residual sediment flux; to determine the contributions of different sediment-transport processes and their variability with discharge; and to discuss the geomorphic implications of the observations.

1.1. Study Region

The Mekong River ranks seventh worldwide in water discharge (550 $km^3\ yr^{-1}$) and eleventh in sediment discharge (110 Mt yr^{-1}) [*Milliman and Farnsworth*, 2011], based on values determined at locations upstream of tidal influence. The wave-influenced, tide-dominated Mekong delta [*Wright*, 1985] comprises much of southern Vietnam (Figure 1). Tides are mixed-semidurnal and mesotidal, with a spring tidal range of about 3.5 m near the mouth (Figure 2), 2 m at Can Tho, 90 km upstream, and 1 m near the Cambodian border, 190 km from the mouth [*Mekong River Commission*, 2014]. The river forms two main distributaries within the delta: the Bassac or Song Hau and the Mekong or Song Tien (Figure 1). These two distributaries ultimately split into eight major channels that discharge into the East Sea (also known as the South China Sea). This study focuses on the Dinh An channel of the Song Hau distributary. The Song Hau accounts for about 41% of the total Mekong water discharge; the Dinh An carries about 70% of the Song Hau discharge and 27% of the total Mekong River flow [*Nguyen et al*., 2008], making it the largest of the eight channels. Typical single-thread Mekong discharge upstream of the delta at Kratie, Cambodia ranges seasonally from 2000 to 40,000 $m^3\ s^{-1}$ (Figure 2). On the Song Hau, discharge magnitude is reduced by branching upstream, and seasonal variation is diminished by the influence of Tonle Sap lake, which acts as a natural flow capacitor that moderates flow within the delta [*Fujii et al*., 2003; *Mekong River Commission*, 2009]. Typical Song Hau discharge ranges seasonally from 5000 to 12,000 $m^3\ s^{-1}$ at Can Tho, Vietnam, 35 km upstream of the landward extent of our study area (Figure 1). During high flow, freshwater can extend to the mouth of the Dinh An, while during low flow, salt water has been observed to penetrate about 50 km landward of the mouth [*Wolanski et al*., 1996, 1998; *Nguyen and Tanaka*, 2007; *Nguyen et al*., 2008], although the river mouth endpoint (i.e., 0 km location) for some of these studies was undefined.

As of 2011, there were 64 dams in the Mekong basin, with another 233 under construction or in planning; the largest of the operational dams are in China [*Xue et al*., 2011]. The influence of damming on the hydrological and sediment-transport regime of the lower Mekong is mixed. Mean flows remain similar to predam periods [*Lu and Siew*, 2006], but the reduced variability due to dams enhances the importance of local precipitation to discharge variations [*Xue et al*., 2011]. Although sediment discharge at upstream locations has been reduced considerably by damming, farther downstream it has not significantly changed [*Kummu and Varis*, 2007].

The seasonal monsoon dominates weather in the Mekong delta. Offshore winds and waves come from the southwest during the wet summer monsoon (May–October), while during the drier winter monsoon

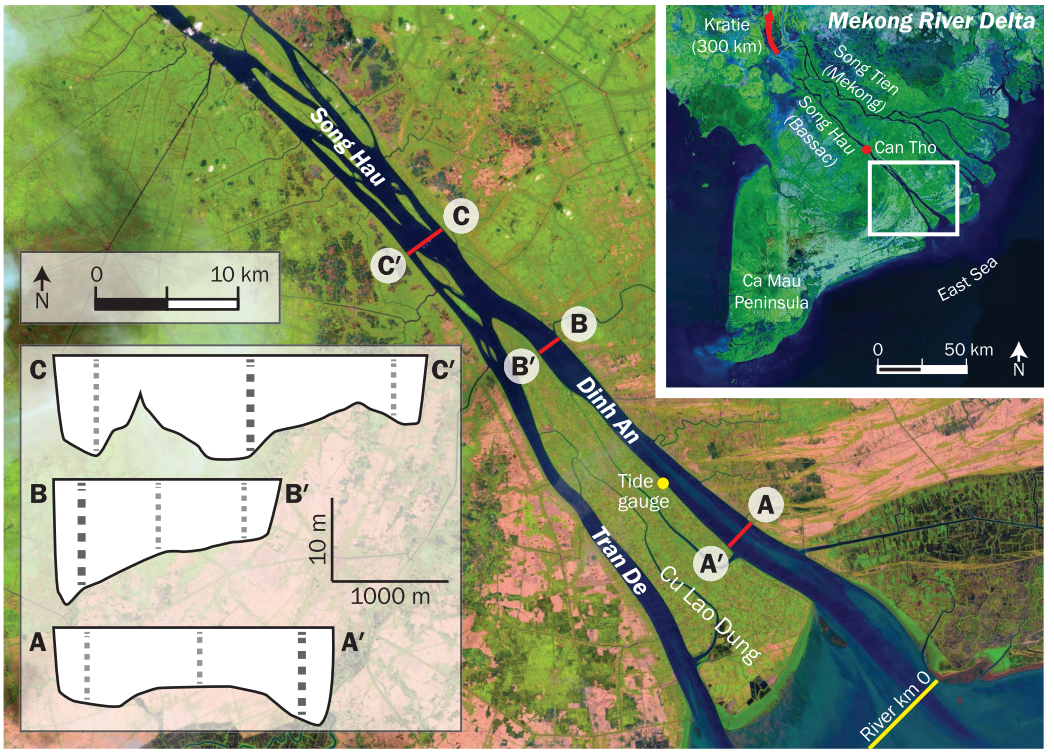

Figure 1. Study area basemap with Landsat 7 ETM imagery acquired 13 February 2002. Red lines denote cross sections occupied during the two cruises, and the yellow dot indicates the location of the tide gauge deployed during this study. The mouth (river km 0) is defined as the cross-channel extension of the left-bank limit. This is seaward of Cu Lao Dung's subaerial extent but representative of the geomorphic transition from river to open ocean given the extensive tidal flats fronting Cu Lao Dung. The inset at bottom left shows generalized bathymetry as viewed downstream, with nominal station locations indicated by dotted vertical lines. The inset map at top right shows the greater Mekong River Delta region, with the locations of the long-term gauging stations at Can Tho and Kratie indicated.

(November–March) winds and waves are greater and from the northeast [*Hu et al.*, 2000]. Shore-parallel shelf circulation near the channel mouths is weak and to the northeast during the summer, and is stronger and to the southwest during the winter [*Gagliano and McIntire*, 1968]. Net transport of sediment is to the southwest [*Gagliano and McIntire*, 1968] and has formed the Ca Mau peninsula and a shelf clinoform [*Ta et al.*, 2005; *Xue et al.*, 2010]. Despite sometimes energetic shelf conditions, waves within the distributary channels were minimal during our field campaigns.

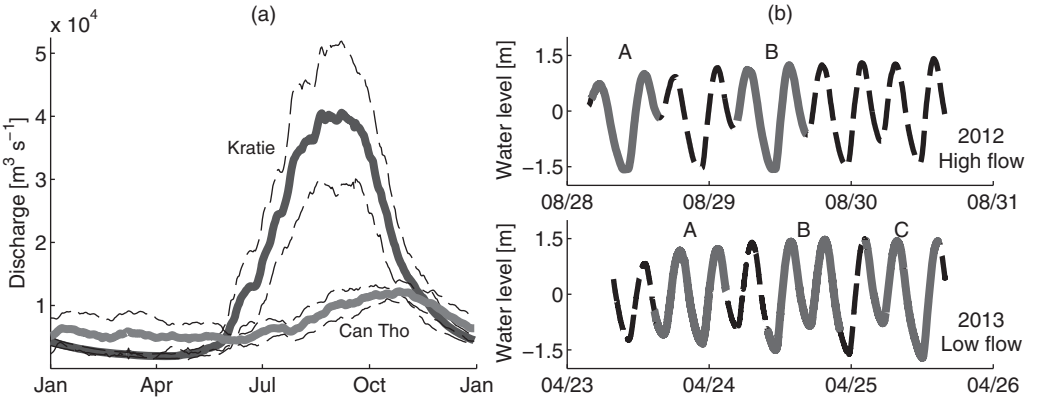

Figure 2. (a) Average historical discharge, ± one standard deviation, at Kratie, Cambodia, based on 45 years of record (1925–1969), and at Can Tho, Vietnam, based on 7 years of record (2001–2007). Data provided by the Mekong River Commission. (b) Measured water level during the 2012 high-flow (top) and 2013 low-flow (bottom) cruises with measurement periods for the cross sections indicated by solid lines. The location of the tide gauge is indicated in Figure 1.

Relatively little previous work has been published on the hydrodynamics and sediment dynamics of the tidal Mekong River. During a high-flow period in 1993, *Wolanski et al*. [1996] encountered salt-wedge estuarine conditions where ebb flows were stronger than floods, no along-channel SSC gradient was observed, no turbidity maximum was present, and the river bed was mostly sandy. They further found that deposition and erosion dominated SSC variability and the system exported sediment to the ocean. During low flow in 1996, *Wolanski et al*. [1998] observed a system that was partially mixed with stronger peak flood flows than ebb flows. In that study, suspended sediment, possibly deposited offshore during previous high-flow periods, was posited to be transported landward from coastal waters.

2. Methods

2.1. Data Collection

Vessel-based surveys of flow velocity, salinity, suspended-sediment concentration, and river-bed sediment were made during high-seasonal and low-seasonal discharge in August–September 2012 and in April 2013, respectively. A 600 kHz RD Instruments acoustic Doppler current profiler (ADCP) measured flow velocity. An RBR, Ltd. XRX-620 CTD with integrated optical backscatter sensor (Campbell Scientific OBS-3+), both sampling at 6 Hz, measured profiles of salinity, temperature, depth, and suspended-sediment concentration (SSC). Water samples were collected in situ for the purpose of calibrating the OBS to SSC. Bed sediment was collected with a grab sampler.

Our field efforts captured the seasonal and spatial variability of the Song Hau and its distributary channels. Observations were made at three cross sections (Figure 1), two of which—sections A and B, in the Dinh An channel—were reoccupied during both campaigns. Section C, on the Song Hau and upstream of the bifurcation around the island of Cu Lao Dung, was occupied only during low flow. Channel bathymetry is complex and varies between sections (Figure 1). Section A consists of two deep channels separated by a mid-channel shoal. Section B has a deep thalweg close to the left bank and the bathymetry gradually shoals toward the right bank. Section C is made up of three channels separated by shoals that are extensions of islands immediately upstream and downstream of the cross section. The left and center channels are directly connected to Dinh An, and the right channel is more directly connected to Tran De.

At each section, the ADCP operated continuously for about 24.8 h. The vessel repeatedly traversed each cross section and completed a one-way pass in 15–30 min, depending on channel width, other vessel traffic, and logistical considerations. At each section, stops were made on alternate crossings at three predetermined station locations (Figure 1) to conduct CTD casts and collect water samples. Bed-sediment samples were collected at each section throughout the tidal cycle.

2.2. Data Processing

The data were quality checked and spurious data points were removed. No-data areas from instrument blanking near the water surface and river bed were extrapolated by prescribing a no-slip condition at the bottom and applying a shape-preserving cubic spline to the empty regions. CTD data extended closer to the surface and bed than the ADCP data, but any gaps in the CTD data were filled by linear extrapolation. Representative ADCP data were assigned to each CTD cast by averaging 200 m of ADCP data centered around each CTD station. Throughout this paper, velocities and fluxes are presented in a channel-wise coordinate system using the fluvial convention: positive along-channel values indicate downstream flow, and positive across-channel values indicate flow toward the right bank.

Water samples were filtered on board, and were dried and weighed to compute SSC during measurements at each section. The voltage output of the OBS was calibrated by regressing against the measured SSC for each of the cruises. The quality of the OBS calibration was good, with R^2 values of 0.74 during the high-flow cruise and 0.80 during the low-flow cruise.

Wet bed-sediment samples were disaggregated using a 0.05% $NaPO_3$ dispersant solution and sonicating bath. The disaggregated samples were wet sieved into fine (<63 μm; silt and clay) and coarse (>63 μm; sand) fractions. Grain size of the disaggregated fine fraction was determined with a Micromeritics SediGraph

III particle-size analyzer, and the full distribution was compiled by using the ratio of the dry masses for the fine and coarse fractions.

2.3. Sigma Coordinates and Decomposition

To help interpret seasonal and spatial variability, we averaged the velocity and sediment fluxes over the 24.8 h tidal cycles and also decomposed the subtidal sediment fluxes. In this process, we replaced depth values with a fixed number of sigma levels that vary between 0 at the water surface and 1 at the bed. Sigma coordinates are particularly useful in shallow settings with large tidal ranges [*Giddings et al*., 2013] like the Mekong. Cross sections were divided into a fixed quantity of grid cells of area dA by applying sigma coordinates across the width of each section. The magnitude of dA varies as the cross-sectional area changes with the tide, but the number of elements remains constant.

The tidally averaged but spatially varying flux field is

$$\langle u(y,\sigma,t)\, c(y,\sigma,t)\rangle, \tag{1}$$

where u is velocity, c is concentration (e.g., of salt or sediment), and angle brackets denote a tidally averaged quantity. Both u and c vary across-channel (y), vertically (σ), and in time (t). When considering the residual velocity alone, c is set to 1 everywhere.

The subtidal or residual flux through a cross section is

$$F=\left\langle \int uc\, dA \right\rangle, \tag{2}$$

which is the section-integrated form of equation (1). When considering salinity, F will be zero for an estuary in steady state, though steady state is rarely achieved [*Uncles et al*., 1985a]. F is generally nonzero for sediment, suggesting import or export. This is because sediment can have local sources and sinks via resuspension and settling, and generally does not escape upriver to its terrestrial source as salt can escape to its ocean source. For $c = 1$, F is water discharge.

We decomposed the flux following the method described by *Lerczak et al*. [2006]. This routine opts for simplicity by grouping into only three terms: a sectionally and tidally averaged term, a sectionally varying and tidally averaged term, and a remainder term, which is sectionally and tidally varying:

$$\begin{aligned} F=\left\langle \int uc\, dA \right\rangle &= u_0 c_0 A_0 + \int u_1 c_1\, dA_0 + \left\langle \int u_2 c_2\, dA \right\rangle \\ &= F_R + F_E(\sigma) + F_T(y,\sigma). \end{aligned} \tag{3}$$

In the equation above, $u_0=\left\langle \int u\, dA \right\rangle / A_0$, $c_0=\left\langle \int c\, dA \right\rangle / A_0$, $A_0=\left\langle \int dA \right\rangle$, $u_1=\left\langle u\, dA \right\rangle / dA_0 - u_0$, $c_1=\langle c\, dA\rangle / dA_0 - c_0$, $u_2=u-u_0-u_1$, and $c_2=c-c_0-c_1$. Full details of the derivation can be found in *Lerczak et al*. [2006] and *MacCready and Banas* [2011]. This mathematical procedure makes no assumptions about estuary or tidal-river properties. Accordingly, the terms must be interpreted with care. The first term, F_R, is attributed to seaward advection of material by the river flow, potentially to a location outside the mouth, and includes Stokes drift. The second term, F_E, is the flux associated with particle movement via estuarine exchange-flow flux. Tidally averaged velocity and salinity fields can be inspected to see whether this term in fact results from gravitational circulation. The remainder is F_T, often called the "tidal term," which arises from temporal correlations of velocity and the constituent. F_T contains all other processes, including tidal pumping and, in the case of sediment, local erosion and deposition.

3. Results

Data from measurements at the three cross sections show that the Dinh An channel was an ebb-dominant tidal river with an ephemeral salt wedge during high flow and a flood dominant, partially mixed estuary during low flow. Table 1 gives an overview of the conditions during the two cruises. Spring and near-spring tides were present during both cruises, with a maximum tidal range that exceeded 3 m (Figure 2). During the high-flow cruise, diurnal tidal inequality was greatest during measurement at section A; greater and lesser daily tides were similar during measurement at B. Tidal range increased during the low-flow campaign, with the largest tides present during measurement at section C.

Table 1. Velocity Dominance, Estuarine Regime, Tidal Range From Lower Low Water to Higher High Water in m, Salinity Range in PSU, Top-to-Bottom Stratification Range (ΔS) in PSU, 95% Range of Depth-Averaged SSC in mg L^{-1}, and Bed Grain-Size Characteristics During High and Low Flow at Sections A, B, and C

	High Flow		Low Flow		
	A	B	A	B	C
Velocity	Ebb dominant	Ebb dominant	Flood dominant	Flood dominant	Flood dominant
Estuarine regime	Salt wedge/tidal river	Tidal river	Partially mixed	Partially mixed	Partially mixed
Max. tidal range	2.5	2.7	2.4	2.9	3.1
Salinity	0–18	0	8–24	2–12	0–6
ΔS	0.0–18.0	0.0	0.2–13.2	0.0–6.2	0.0–2.8
SSC	62–296	71–172	27–300	35–480	35–573
Bed sediment	Sand/mud	Sand/mud	Mud	Mud	Sand/mud

3.1. High Flow

3.1.1. Section A

The ephemeral salt wedge at section A was an important modifier of the section's velocity, salinity, and SSC patterns. The salt wedge was present during late floods and into early ebbs, and salinity in the section was zero otherwise (Figure 3). On the lesser flood, salinity within the 6 m thick salt wedge reached 18 PSU. On the greater flood, when salt intrusion was limited by the previous strong ebb, the weaker and thinner salt-wedge salinity reached only 7 PSU. At all times, the salt wedge was thickest and longest lived in the deep right channel. When the salt wedge was present, there was strong velocity shear on floods, with seaward flow in the freshwater above the wedge and landward flow within the wedge. SSC within the salt wedge was low, less than 30 mg L^{-1}, except for during the strongest upstream salt-wedge flow, when near-bed SSC was greater (Figure 4).

Outside of the salt wedge—above it when it was present and throughout the water column when it was not—flows were strong, and exceeded 1 m s^{-1}. Ebbs in this freshwater region were longer and faster relative to floods, and the fastest currents were in the right channel. Minimum freshwater SSC was 100–200 mg L^{-1}, but SSC reached 400 mg L^{-1} near the bed during the strongest flows. SSC outside the salt wedge was correlated with velocity, and concentrations were greater on ebbs.

3.1.2. Section B

In contrast to section A, no salinity was present during measurement at section B (Figure 3). Floods were strongest in the thalweg (left station), and ebbs, which were stronger than floods, were greatest in the middle of the channel. As at section A outside the salt wedge, flow direction was uniform throughout the water column, and there was minimal velocity shear. Depth-averaged SSC ranged from 70 to 170 mg L^{-1}

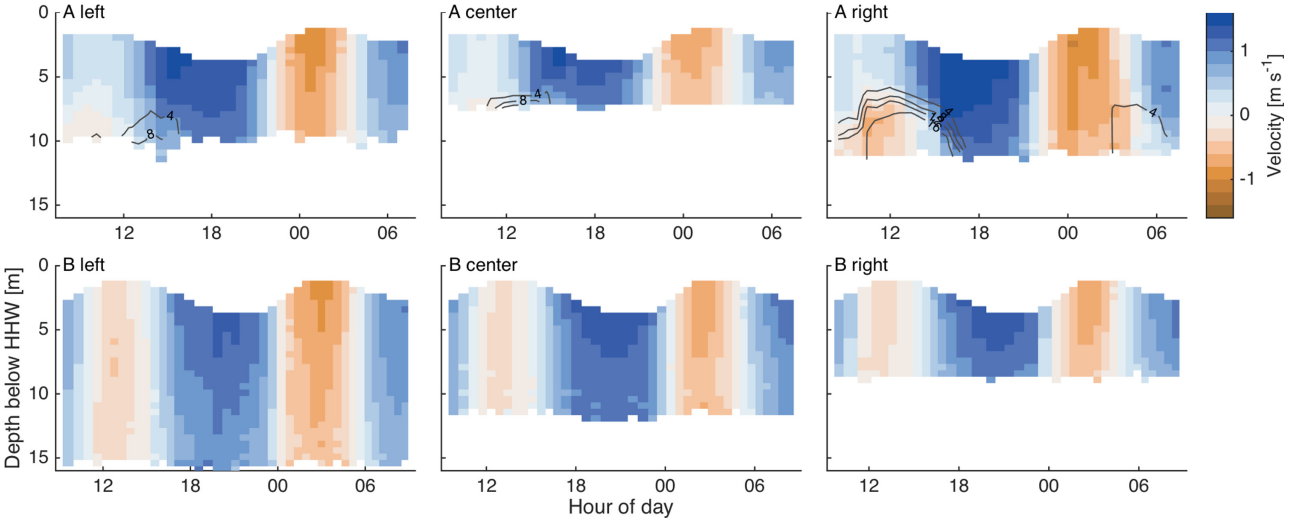

Figure 3. Along-channel flow velocity and salinity during high flow at the left, center, and right stations of (top row) section A and (bottom row) section B. Salinity contour interval is 4 PSU.

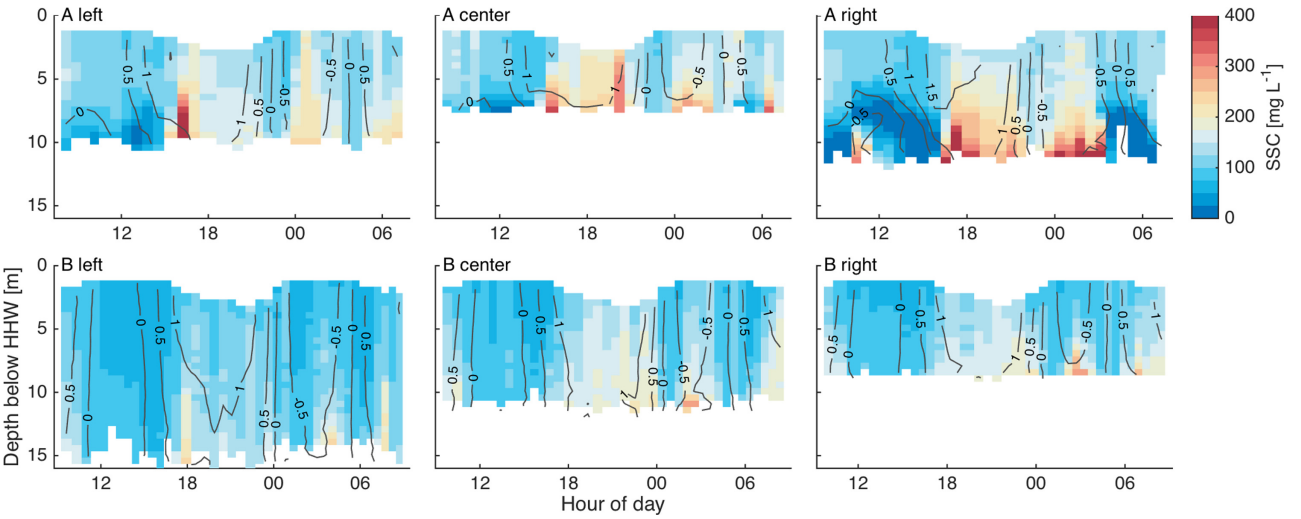

Figure 4. SSC and along-channel flow velocity during high flow at the left, center, and right stations of (top row) section A and (bottom row) section B. Velocity contour interval is 0.5 m s^{-1}.

(Figure 4) and was greater on ebb, similar to the observations at section A. Average SSC at section B was about 30% less than the freshwater regions of section A, though it remained positively correlated with velocity, particularly at the center and right stations, where concentrations were greatest.

3.2. Low Flow

3.2.1. Section A

Flood currents at section A during low flow began first in the lower water column, particularly in the left and right channels. During maximum flood, velocity was upstream everywhere and strongest in the channels (Figure 5). On floods, salinity ranged from 8 to 24 PSU and was partially mixed. Salinity was greatest in the right channel, which is where the salt wedge was strongest during high flow. SSC was vertically heterogeneous and was lesser in magnitude at the center and right stations than the left station, where values approached 700 mg L^{-1} near the bed (Figure 6).

Floods transitioned to ebbs simultaneously throughout the water column, and flow was uniformly downstream everywhere, though slowest near the bed in the right channel. Salinity ranged from 9 to 20 PSU and, as during floods, the greatest values were near the right-channel bed. Stratification was greater on ebbs than floods and ranged from 5 to 10 PSU. As during floods, SSC was least in the right channel and greatest in the left channel, and exceeded 700 mg L^{-1} near the bed during the strongest ebb flows.

3.2.2. Section B

At section B, flow velocity was strongest, salinity greatest (4–8 PSU), and SSC largest (>1000 mg L^{-1}) in the thalweg on flood, though the greatest salinity values were delayed until the end of the flood (Figures 5 and 6). This behavior is consistent with observations in the deeper regions of A, where these quantities were also greatest on floods. A strong correlation between near-bed velocity and SSC was present, especially in the thalweg, and SSC at B was in general greater than at section A.

On ebbs, flow and SSC were greater over the shoal and lesser in the thalweg. Flow velocity was nearly 1 m s^{-1} and SSC exceeded 1000 mg L^{-1} near the bed at the right station but remained less than 300 mg L^{-1} in the thalweg. As during floods, salinity was greatest in the thalweg, and ranged from 4 to 9 PSU.

3.2.3. Section C

At section C, dynamics in the left and center channels were similar but distinct from those in the right channel. On floods, flow was stronger in the left and center channels (1–1.2 m s^{-1}) and weaker in the right channel (0.7–0.8 m s^{-1}) (Figure 5). Salinity was greatest at the left station (3–5 PSU) and least at the right station (∼1.5 PSU). SSC was greatest in the left and center stations, correlated with near-bed flow velocity, and vertically heterogeneous. Average SSC was also greater than the values observed at sections A and B. In the left and center channels, the 1000 mg L^{-1} isolute was about 2 m above the bed and maximum concentrations were about 2500 mg L^{-1}; SSC in the right channel reached only about 400 mg L^{-1} (Figure 6).

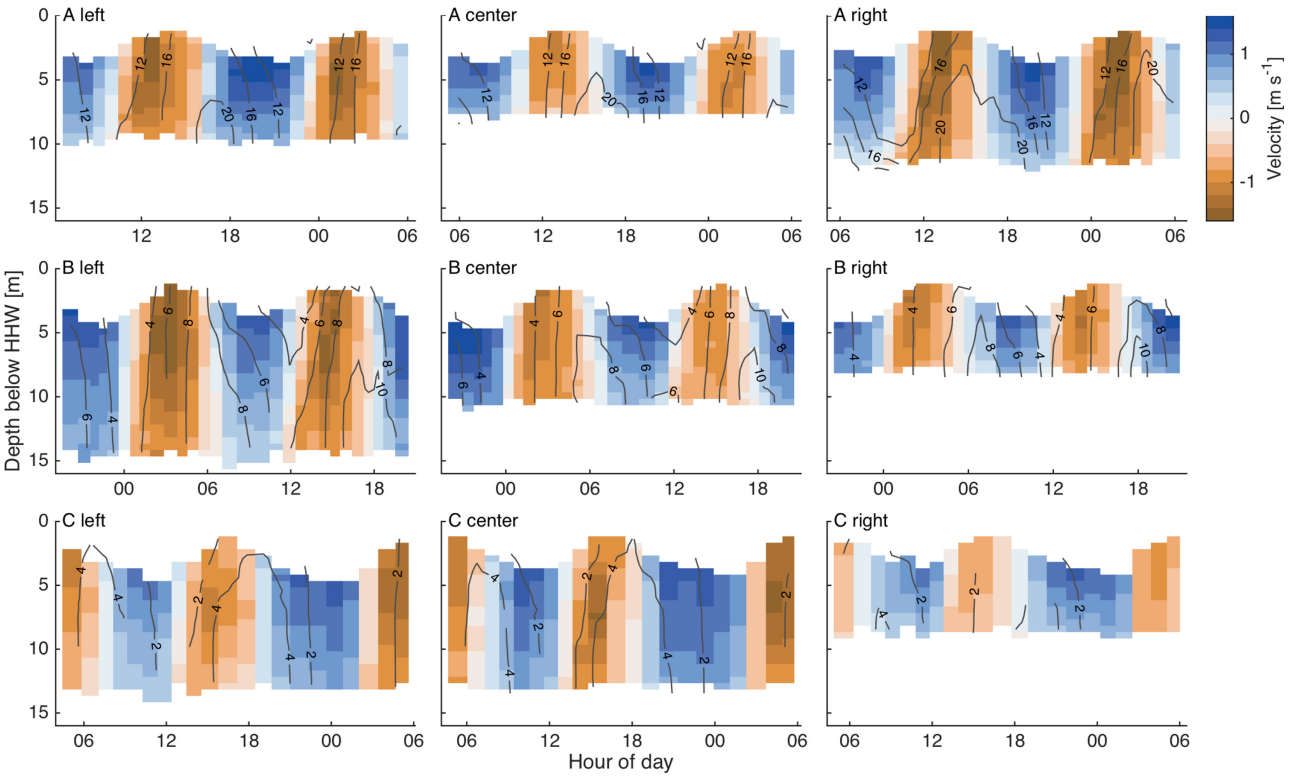

Figure 5. Along-channel flow velocity and salinity during low flow at the left, center, and right stations of (top row) section A, (middle row) section B, and (bottom row) section C. Salinity contour interval varies.

On ebbs, maximum velocity was focused in the thalwegs of the three channels. Salinity ranged from 1 to 2 PSU at all three stations, though it was generally less at the right station than the left and center stations. SSC was generally less than 200 mg L^{-1}, but was correlated with velocity, especially in the right channel, where ebb SSC was greatest.

3.3. Bed Sediment

The bed-sediment distributions were distinct between the two cruises. During high flow, grain-size distributions at the deeper sections of A and B were coarse, with averages at those stations as high as 70% sand by mass (Figure 7), but there was considerable variability among the samples. Mud balls, pebble-like clasts of consolidated mud, are evidence of an erosive bed [*Bell*, 1940], and were prevalent at the left and center stations of B. Samples collected at moderate to deep depths, for example the center station at section B, were variable, potentially suggesting significant spatial heterogeneity in the bed-sediment grain size of those regions. Shallow areas—the center station at section A and right station at section B—were finer, with sand fractions averaging less than 12% by mass.

During low flow, bed sediment at A and B was finer than during high flow, with a sand fraction of about 15% on average at each station (Figure 7). Within-section variability was minimal, in contrast to the spatial heterogeneity during high flow. At section C, grain size at the left and center stations, which are more directly connected to the Dinh An channel than the right station, was coarse and spatially heterogeneous, and was similar to the deep stations of section A and B during high flow. The right station, which is more directly connected to the Tran De channel (Figure 1), was considerably finer, even more so than at A and B during low flow, and averaged only about 5% sand.

4. Discussion

Depending on seasonal river flow, the lower Mekong River transitions from a freshwater tidal river with an ephemeral salt wedge to a partially mixed estuary. Here we interpret this seasonal regime change, compute

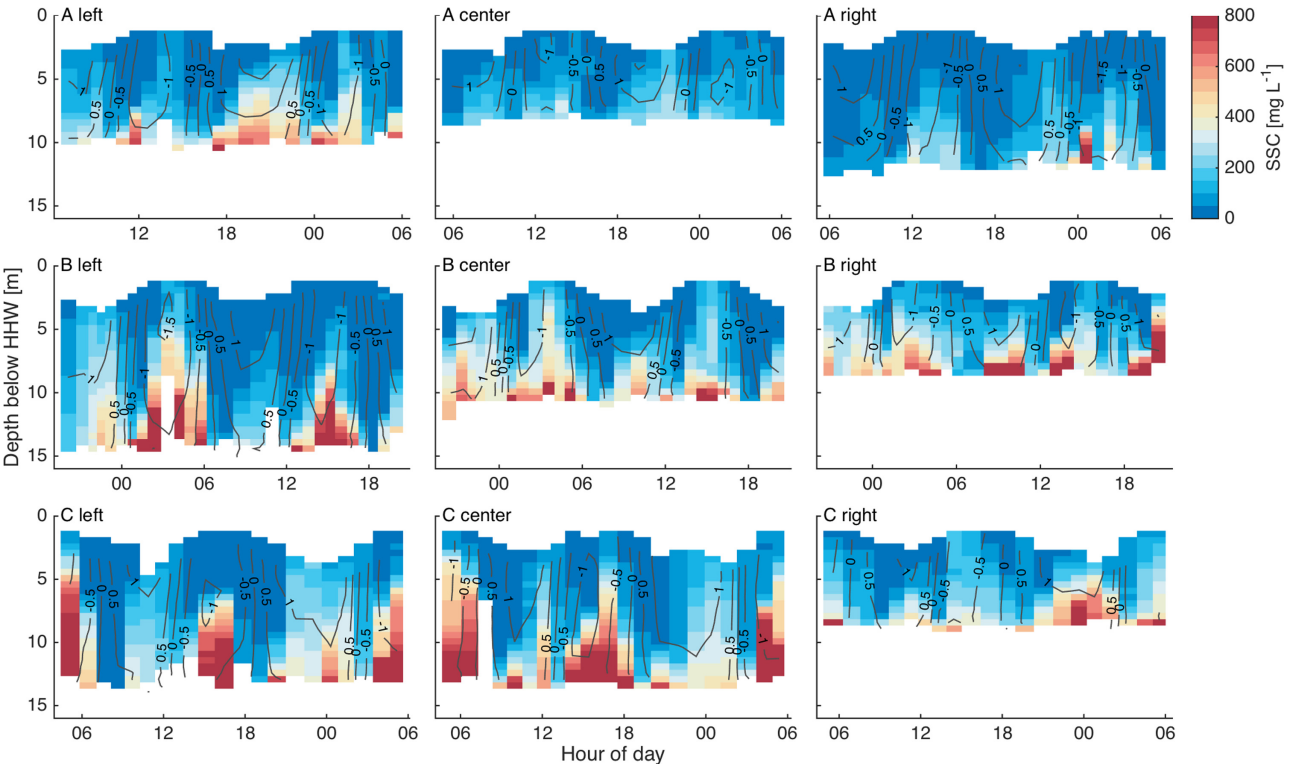

Figure 6. SSC and along-channel flow velocity during low flow at the left, center, and right stations of (top row) section A, (middle row) section B, and (bottom row) section C. Velocity contour interval is 0.5 m s^{-1}.

patterns of residual velocity and sediment flux, review factors that control these patterns and consider their significance, and provide insights on the geomorphic response of the system.

4.1. Seasonal Regime Change

4.1.1. Freshwater Discharge

During high flow, instantaneous water discharge reached a maximum of more than 20,000 m^3 s^{-1} on ebb tide and about −18,000 m^3 s^{-1} on flood tide (Figure 8). After integrating the instantaneous discharge over the 24.8 h tidal cycle, the resultant freshwater river discharge was approximately 7300 m^3 s^{-1}. Assuming that the Dinh An channel represents about 70% of Song Hau discharge [*Nguyen et al*., 2008], total Song Hau discharge was about 10,000 m^3 s^{-1} during the high-flow cruise. Although modern discharge records are limited, this scaled discharge compares favorably to the 2001–2007 average Song Hau high-flow discharge measured at Can Tho (Figure 2).

During low flow, maximum discharge at sections A and B was about 20,000 m^3 s^{-1} on ebb and about −25,000 m^3 s^{-1} on flood. Mean discharge was only about 500 m^3 s^{-1} at A and B during the low-flow cruise, a factor of 50 smaller than the maximum instantaneous discharge values. At section C, both ebb and flood discharge magnitudes were greater than at A and B, exceeding 22,000 and −30,000 m^3 s^{-1}, respectively, and the mean freshwater discharge was about 1200 m^3 s^{-1}. The ratio between discharge at sections A and B and that at section C during low flow was thus about 40%, which is somewhat smaller than the estimate of *Nguyen et al*. [2008]. The greater discharge results from the location of section C: it is upstream of Cu Lao Dung and spans the width of the Song Hau before the Song Hau branches into the Dinh An and Tran De channels (Figure 1). This estimate suggests that discharge during the low-flow cruise was about one standard deviation below the historic low-flow discharge measured at Can Tho (Figure 2). Put into the context of previous studies, Dinh An low-flow discharge was less than the 1200 m^3 s^{-1} reported by *Wolanski et al*. [1998] during their low-flow study in April 1996 but was similar to the 650 m^3 s^{-1} reported by *Nguyen et al*. [2008] for a period in April 2005. The agreement with *Nguyen et al*. [2008] for low-flow Dinh An discharge did not extend to the full Song Hau, however, where the 2005 estimate was 920 m^3 s^{-1}, about 25% smaller

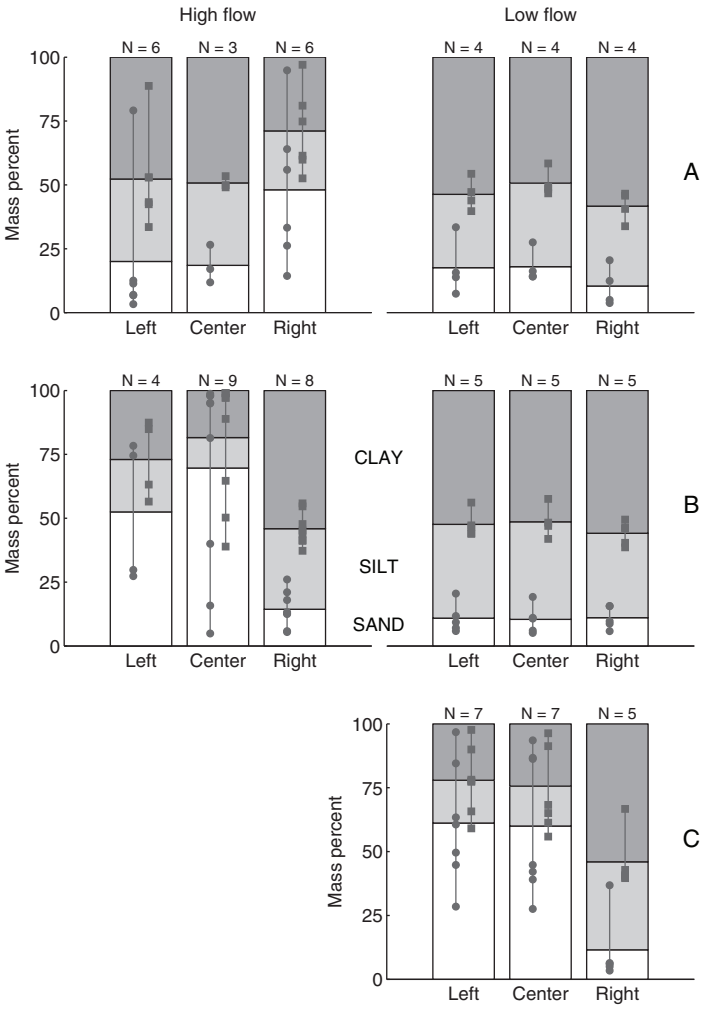

Figure 7. Mean sand, silt, and clay bed-sediment mass distributions at sections A, B, and C during high and low flow. Sample ranges are plotted as dots (sand-silt boundary) and squares (silt-clay boundary) connected by vertical lines. The number of samples analyzed at each location is listed at the top of each distribution. There was considerable seasonal variability in grain size at sections A and B, and marked cross-channel variability in grain size was present during high flow at A and B and low flow at C.

than the value measured at section C in the present study. Nevertheless, the freshwater discharge during both cruises fell within typical seasonal ranges, enabling further discussion of the changing flow regimes.

4.1.2. Velocity Patterns

The dominant tidal-flow direction is a function of the freshwater that must be carried downstream by the river, and the magnitude of ebb dominance increases as river flow grows relative to the flow induced by filling and draining the tidal prism [*Savenije*, 2005]. Unless the river floods its banks, ebbs will be stronger and of increased duration during high river discharge to accommodate the additional freshwater input. During high flow, river discharge was so great that the spatial majority of section A continued flowing seaward even during the lesser flood (Figure 3); this behavior, along with the extended-duration ebbs, helped flush suspended-sediment downstream. During low flow at A and B, when the river discharge was small compared to the tidal prism, floods were stronger than ebbs. The flow-velocity patterns at C were a hybrid of the more riverine (high flow) and more tidal (low flow) conditions at A and B. During low flow, the greater freshwater discharge at section C produced high-flow characteristics like extended ebb duration, while still being flood dominated (Figure 8). At section C, located just upstream of the split into the two distributary channels, flow in the right channel was less flood dominated than in the left and center channels, suggesting that flood tides were preferentially routed via the Dinh An channel and ebbs via the Tran De channel (Figure 5).

4.1.3. Salinity Intrusion

Salinity intrusion length was computed at the three stations of each cross section by time-integrating the velocity field on floods from the time when salinity rose above zero until high slack water. This gives an approximate upstream location of the maximum landward salinity intrusion in the absence of significant along-channel data coverage for a given tidal cycle. Using this method, the salt wedge intruded 11 km upstream of section A on the high-flow greater flood. This location, some 30 km upstream of the mouth (river km 0; Figure 1) and 8 km downstream of B, is farther landward than the location of maximum salinity intrusion found by *Wolanski et al.* [1996]. That study took place in November, when Song Hau discharge is on average about 10% higher than during our study period, suggesting that, despite extensive dam construction in the interim [*Xue et al.*, 2011], the high-flow salinity intrusion length has not changed dramatically in the past 20 years. The stability of the salinity intrusion length may be related in part to the

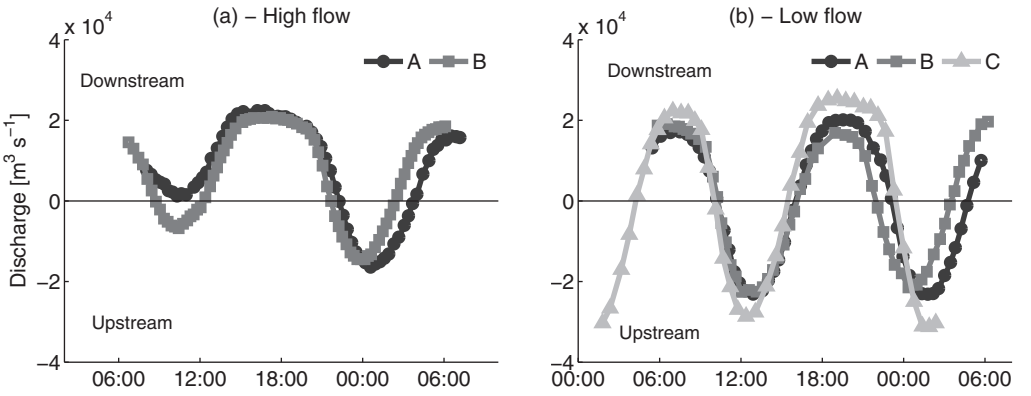

Figure 8. Instantaneous water discharge at sections A, B, and C during (a) high flow and (b) low flow. The data have been time shifted and overlaid to allow for easier comparison. Ebbs were of increased duration and stronger than floods during high flow, and floods were stronger than ebbs during low flow; tidal fluctuations were much greater than the mean discharge during both conditions.

moderating influence of Tonle Sap on flow downstream [*Fujii et al.*, 2003; *Mekong River Commission*, 2009], together with the importance of lowland precipitation (i.e., below significant damming) to water discharge in the Mekong delta. During the greater ebb, salinity was pushed 13 km downstream of section A, about 3 km landward of river km 0 (Figure 1), again based on integration of the velocity field at section A.

Maximum salinity intrusion during the low-flow cruise was 22 km upstream of section C, and 55 km upstream of the mouth, about half way to Can Tho. This value is similar to previous estimates of salinity intrusion during low flow of 45–60 km [*Wolanski et al.*, 1998; *Nguyen and Tanaka*, 2007; *Nguyen et al.*, 2008], despite different freshwater discharge between those investigations and the present study. On ebbs, salinity was pushed about 1 km downstream of section C at the left and center stations and about 3 km downstream at the right station. The difference in salinity intrusion locations is further evidence (in addition to the previously discussed velocity patterns) that during low flow, ebbs are preferentially routed via the Tran De channel, and floods are preferentially routed via the Dinh An channel.

4.1.4. Suspended-Sediment Resuspension and Advection

During high flow, SSC in freshwater regions—section A outside the salt wedge and everywhere at section B—was correlated with velocity on both floods and ebbs (Figure 9), with higher values on ebb owing to the stronger ebb velocities. The salt wedge at A shielded the river bed from high bed stresses, and SSC in the salt wedge was substantially lower than in the freshwater regions, except during periods of strongest upstream flow within the salt wedge (Figures 3 and 4), when local resuspension occurred. Saline water from offshore entering the river channel was generally devoid of sediment; if it carried any sediment in suspension when offshore, that sediment settled out by the time it reached section A. The low SSC in the

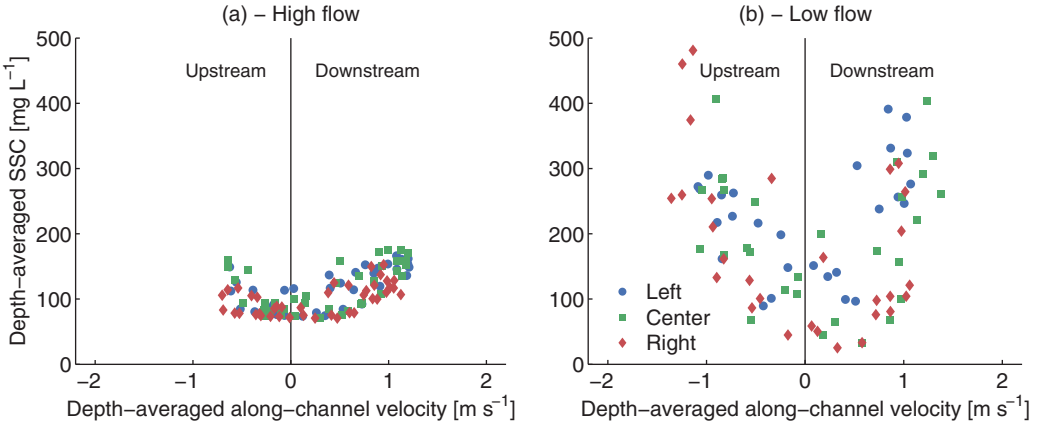

Figure 9. Depth-averaged flow velocity plotted against depth-averaged SSC at section B during (a) high flow and (b) low flow. Greater SSC was associated with stronger velocities; the SSC range was constrained during high flow and was considerably expanded during low flow.

saline water is congruent with the weak southwesterly waves and low winds at the coast during the summer monsoon [*Hu et al*., 2000], though the shallow depth (~5 m) of the subaqueous delta topset [*Unverricht et al*., 2013] suggests that even moderate waves could resuspend sediment there.

Minimum SSC was greater during high flow than low flow in the freshwater regions (Figure 9). The enhanced minimum SSC during high flow suggests that delivery from upstream was considerable, and sediment settling rates were slow in freshwater regions, likely because flocculation of riverine sediment was limited in regions of low salinity. *Wolanski et al*. [1996] posited that advection could be disregarded and variability in the sediment signal during high flow was fully attributable to local erosion and deposition. Although our data similarly show that the (minor) SSC variability is primarily due to local erosion and deposition, the majority of the fine-grained sediment transported during high flow is carried by the river from locations upstream.

SSC during low flow was more dynamic: minima were lesser and maxima were greater than during high flow (Table 1). This was in part because of flocculation enhanced by the presence of salinity [*Postma*, 1967] throughout the tidal cycle at A and B. In addition, more fine-grained sediment was available on the river bed to be resuspended (Figure 7), and the strong vertical variation in SSC (Figure 6) shows that this sediment was not fully mixed throughout the water column. The vertical SSC heterogeneity, in conjunction with the relatively strong velocity shear, suggests preferred sediment pathways within the water column wherein sediment is brought landward lower in the water column and seaward in the upper water column [*Meade*, 1969]. Depth-averaged concentrations tended to be higher on the flood (Figure 9b) which, when combined with the flood-dominant flow velocity, fostered landward sediment pumping. The low background SSC, large resuspension signal, and flood dominance suggest that sediment delivery from upstream was minor compared to local processes.

4.2. Residual Flow and Sediment Flux

4.2.1. High Flow

During high flow at sections A and B, the residual velocity was downstream everywhere (Figure 10), resulting from the significant freshwater input to the system. The minimum in residual velocity near the bottom of the deeper right channel at A was due to upstream flow in the ephemerally present salt wedge (Figure 3). In a purely fluvial system, the maximum residual velocity would be in the thalweg. In this tidal-river reach, however, the lowest residual velocity at B was in the thalweg within 500 m of the left bank, and the maximum was in the middle of the cross section. The velocity minimum could be related to salt-wedge effects from locations downstream influencing flow at B, even though salinity at B never exceeded 0.1 PSU. The residual velocity minimum in the thalweg could also be from the interaction of shallow-water overtides resulting in stronger floods in deep sections and stronger ebbs in shallow sections. The reduced ebb dominance in the thalweg contrasts sharply with the fluvial case, and highlights one of the fundamental differences between tidal and nontidal rivers. Furthermore, the similarity between flows in the deep thalweg on the left-hand side of B and those in the right-hand channel of A suggests that these locations are hydraulically connected, highlighting the system's complex bathymetry.

Residual sediment flux during high flow echoed the residual velocity. At section A, the seaward residual sediment flux (Figure 11) is expected because of the downstream velocity field (Figure 10) and low SSC variability (Figure 9). The residual velocity drove the strongest residual sediment fluxes in the intermediate water column of the deep regions to the left and right of the mid-channel shoal, and toward the right side of the mid-channel shoal (Figure 11). The smallest residual sediment flux, close to the bed in the right channel, was a result of the intermittently present salt wedge there, which was slow moving and generally devoid of sediment (Figures 3 and 4). At B, sediment discharge was similarly downstream everywhere. The greatest downstream flux per unit area was over the shoal, and the flux in the thalweg was weaker. The reduced sediment flux in the thalweg is consistent with the lower SSC and reduced residual velocity (Figure 10) there. In summary, the residual fluxes during high flow reveal the spatially heterogeneous sediment pathways of tidal rivers as compared to their nontidal, fluvial counterparts.

4.2.2. Low Flow

During low flow, the zones of residual upstream flow in the deep areas of A and B (Figure 10) were compensated by downstream flow in shallower regions, a pattern that arose from the influence of gravitational circulation. As is the case for the instantaneous velocity, the residual flow patterns at A and B during high

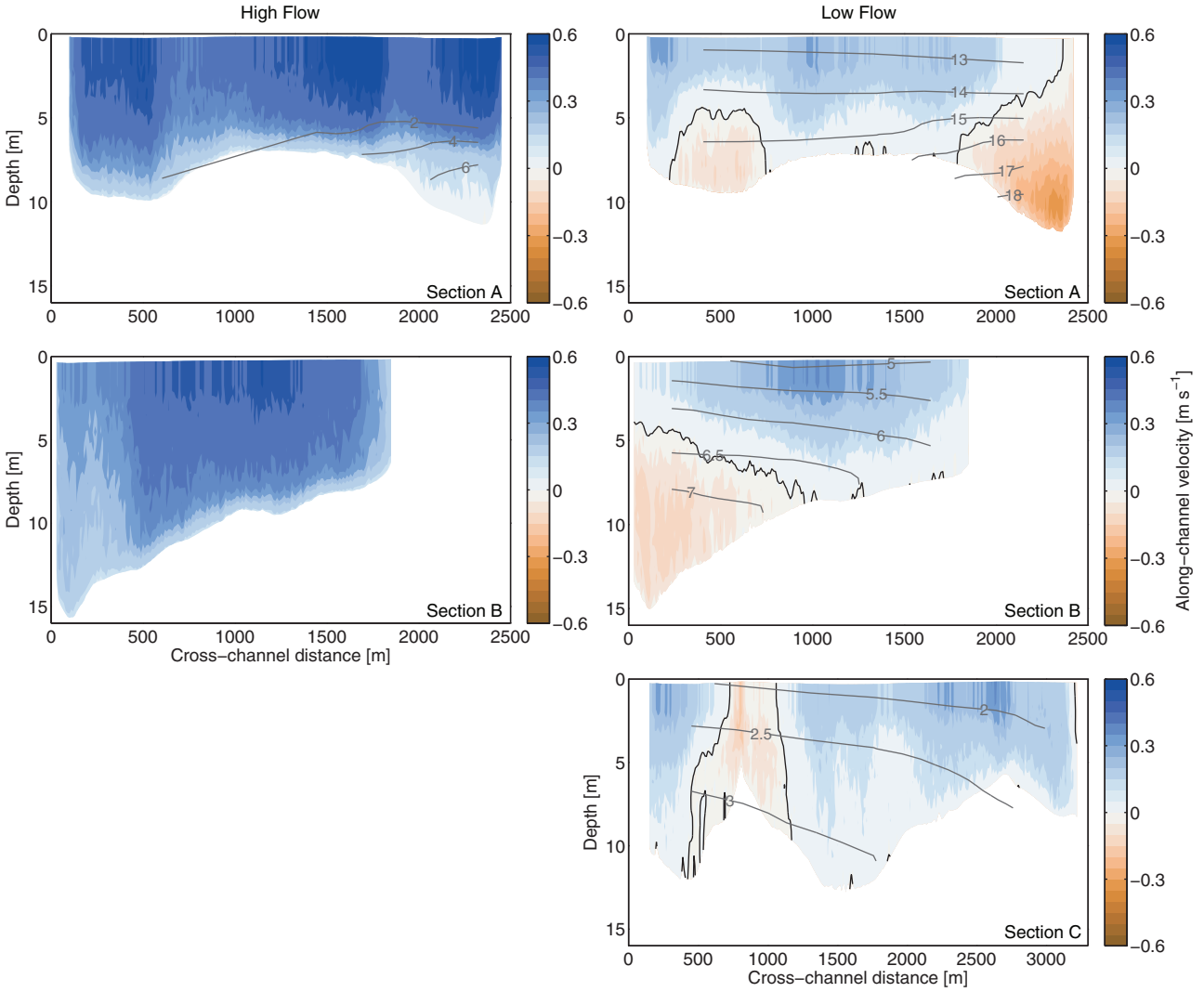

Figure 10. Residual along-channel flow velocity (left) at sections A and B during high flow and (right) at A, B, and C during low flow. Black contour lines indicate velocity zero crossing. Grey, labeled contour lines indicate extrapolated and tidally averaged salinity in PSU. Note change in *x*-axis scale of section C. During high flow, the residual velocity field was downstream everywhere and was focused in intermediate water depths. During low flow, the residual velocity was upstream near the bed and downstream near the surface, with considerable cross-channel variation.

flow and low flow highlight the regime change of the system in response to changing seasonal discharge. Farther upstream, the greater influence of fluvial discharge at C was evident in the downstream residual flow across the majority of the cross section there. Instead of being caused by gravitational circulation, the small region of landward residual flow (Figure 10) resulted from a recirculation zone in the lee of the island just upstream of section C.

In contrast to the high-flow observations, the low-flow residual sediment-flux patterns were at times distinct from the low-flow residual velocity. At both A and B, baroclinic effects resulted in residual sediment flux that was generally landward in the lower portion of the water column and seaward in the upper portion of the water column (Figure 11). In this regard, the sediment pathways were analogous to a coastal-plain estuary [*Meade*, 1969]. Indeed, the increased landward flux in the right channel at A and the thalweg at B mirrored the strong landward residual velocity (Figure 10) and was primarily attributable to the estuarine circulation. Lesser SSC and weaker gravitational circulation in the left channel at A and the shallower regions of B drove reduced landward sediment flux in the left channel and over the mid-channel shoal. The strong landward flux in the deep regions suggests that the preferential landward pathway of sediment import is via the deepest regions, including the right channel at A and thalweg at B. Sediment flux at C, like the

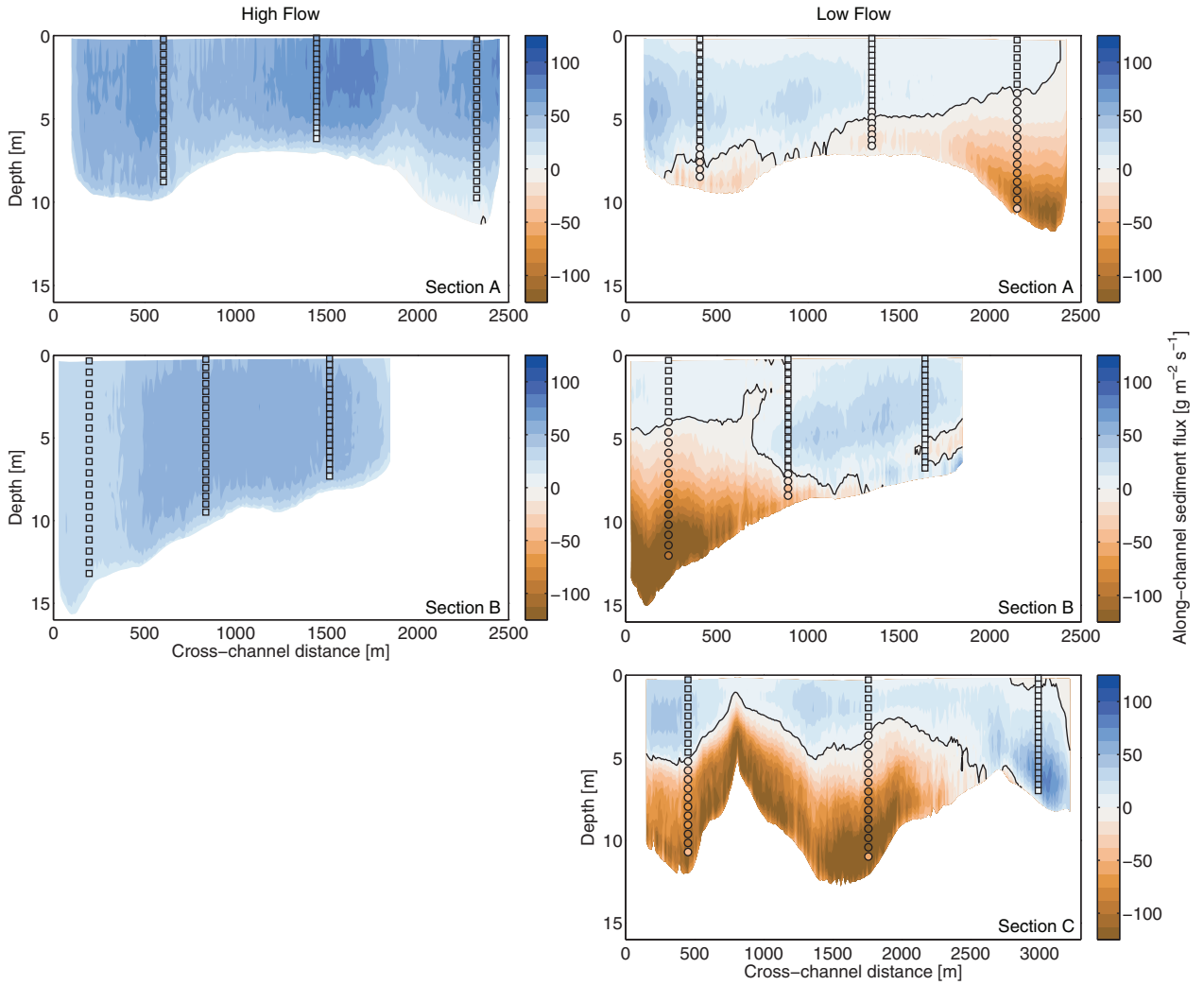

Figure 11. Residual along-channel sediment flux (left) at sections A and B during high flow, and (right) at A, B, and C during low flow. SSC measured at the three stations was extrapolated across the channel and multiplied by the measured velocity to produce these maps. Results from the three stations at each section are presented using circles and squares, with squares denoting seaward flow. Contour lines indicate flux zero crossing. Note change in *x* axis scale of section C. As with residual velocity, the residual sediment flux during high flow was downstream everywhere. During low flow, sediment flux in the upper water column generally was downstream, but there was also considerable upstream residual sediment flux in the lower water column.

residual velocity, was complex, owing to its geographic location immediately upstream and downstream of two mid-channel islands (Figure 1). In contrast to the sediment-flux patterns dominated by gravitational circulation at A and B, the vertical shear in the residual flux of the left and center channels (Figure 11) was likely due to tidal pumping, as the residual velocity at these locations generally was downstream (Figure 10).

The spatial complexity of the low-flow sediment-flux field is consistent with observations in other strongly tidal systems. The pattern of residual downstream sediment flux at the right channel of section C, taken in context with the geographic location of C and the residual velocity characteristics, suggests that during low flow the Dinh An channel (on the left side of C) primarily imports sediment upstream along Cu Lao Dung. In contrast, the Tran De channel, on the right side of C, serves primarily to export sediment from the Song Hau distributary. These characteristics suggest that mutually evasive flow and sediment-flux patterns [*Harris*, 1988] develop around Cu Lao Dung during low flow. Such spatially complex and mutually evasive flow patterns have been observed in other large estuaries and deltas, including the Hudson [*Ralston et al*., 2012], Ganges-Brahmaputra [*Barua*, 1990] and Fly [*Harris et al*., 2004], and modify the release of sediment to the marine environment. Taken together, these studies reinforce the importance of spatially characterizing the sediment and flow field of an entire cross section, and demonstrate the caution that must be taken when flux measured at a single location is extrapolated to a cross section.

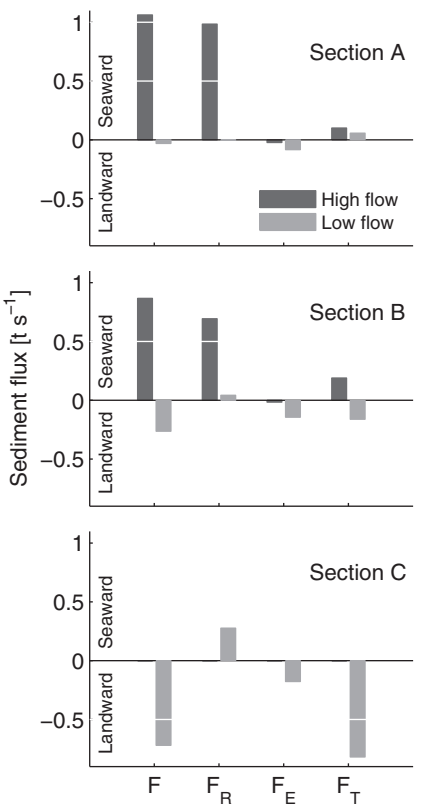

Figure 12. Decomposed residual sediment fluxes at sections A, B, and C during the two cruises. Section C was measured only during low flow. *F*: total flux; F_R: river flux; F_E: exchange-flow flux; F_T: tidal flux. The total flux was downstream and dominated by F_R during high flow; it was upstream and had large contributions from F_E and F_T during low flow.

4.3. Factors Controlling Sediment Discharge

Applying equation (3) enables decomposition of the residual sediment flux into terms that represent physically meaningful processes. This procedure allows for an improved interpretation of the factors driving the transition from tidal river and salt-wedge conditions to partially mixed estuarine conditions.

We expect the integrated residual sediment flux (equation (2)) during high flow to be seaward at both A and B given the residual velocity and sediment-flux patterns at those locations (Figures 10 and 11). Indeed, the total integrated flux during high flow was seaward at a rate of about 1 t s^{-1} (Figure 12). River advection as characterized by F_R (equation (3)) dominated the residual flux and composed over 80% of the total. The bulk of the remainder was contained in the downstream-oriented tidal term, F_T, suggesting that local resuspension was present and helped transport sediment downstream, but that it was less important than advection from upriver. There was minor upstream exchange flux F_E at section A, likely resulting from the episodically present salt wedge; this flux was small because SSC was generally minimal in the salt wedge and mixing was limited by the sharp pycnocline. Decomposed quantities at B were similar, though F_E was negligible because salinity there was always less than 0.1 PSU.

In contrast, the Dinh An channel during low-flow imported sediment at a rate of less than 0.1 t s^{-1} at section A, about a tenth of the 1 t s^{-1} exported during high flow (Figure 12). F_E drove the net upstream flux, far outweighing the small F_R, although the downstream-oriented F_T partially counteracted F_E. This differs from salt-flux dynamics, where F_T is generally oriented upstream [*MacCready and Banas*, 2011] because shallow-water tidal processes (e.g., flood-velocity dominance) tend to pump material landward. Sediment is not a conservative tracer like salt, however, and other processes like resuspension and settling fluxes contribute to this term.

At section B, about 0.3 t s^{-1} of sediment was imported, a moderate increase from the residual flux calculated at section A. The small downstream F_R was compensated by upstream flux from F_E and F_T. The increase in sediment import at B could be a result of the larger tidal range during that survey day compared to the range during measurement at A (Figure 2).

The net upstream sediment flux was about 0.7 t s^{-1} at section C. The downstream F_R, about 0.3 t s^{-1}, was considerably larger than observed at A and B, and was due to the greater freshwater discharge at section C, on the Song Hau, compared to the Dinh An discharge at A and B (Figure 8). F_E was of the same order as that observed at B, and represented about 30% of the total upstream flux. The driver of the increased upstream flux at C was the large F_T, which more than balanced F_R and increased the total sediment import rate. Larger tides during measurement at section C compared to those at A and B could be partially responsible for the magnitude of F_T there.

4.3.1. Synthesis of Factors

During high flow, river advection was the most important component of the net downstream sediment flux. A large F_R is expected given the significant freshwater input, and the minimal influence of F_E is similarly intuitive because salinity is lacking. Tidal fluxes, including local resuspension and settling, were large compared to the low-flow period but insignificant compared to the high-flow total. During low flow, F_E and F_T were most important, especially in the Dinh An channel. The residual low-flow velocity and salinity (Figure 10) are consistent with a strong F_E driven by gravitational circulation: upstream flow deep in the water column and downstream flow in the upper water column. The strong resuspension during low flow

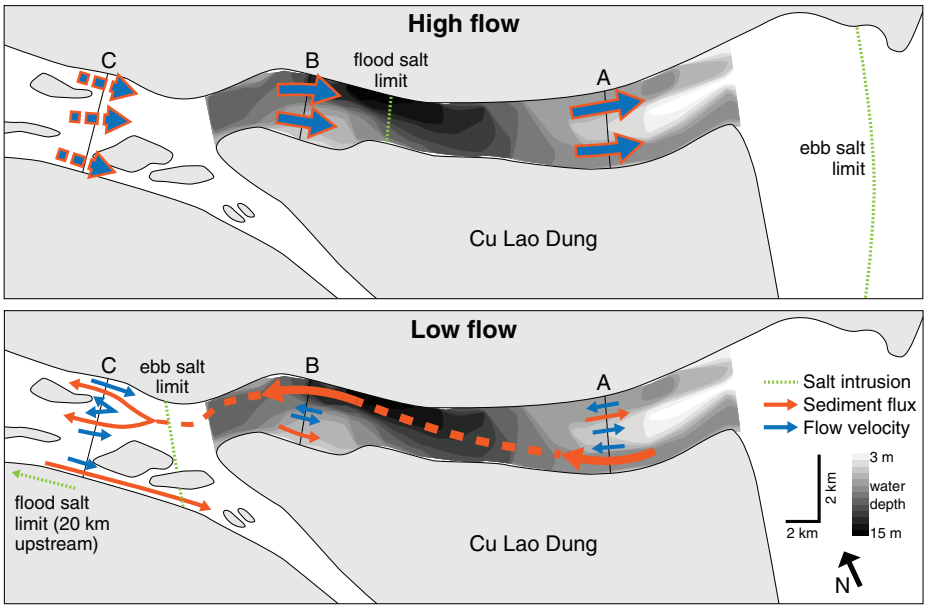

Figure 13. Schematic of residual sediment-transport (orange arrows) and flow (blue arrows) pathways during high and low flow. Thickness of arrows qualitatively indicates flux magnitude. Dashed lines indicate inferred pathways. Salt intrusion extent is calculated by integration of the velocity field and represents the seaward-most locations of water with salinity less than 0.5 PSU. To show pathways better, the scale of this schematic has been distorted. Generalized bathymetric contours are shown for the Dinh An channel.

(Figure 9) and minimal river discharge both enable a large F_T. On the main stem Song Hau at section C, F_R was larger than at A and B because of the greater river flow in that section, but F_E and F_T still drove the net sediment import.

Though we captured large-amplitude tides during our study (Figure 2), they represent a limited subset of the spring-neap progression. Spring-neap tidal variability should not be overlooked [e.g., *Allen et al.*, 1980], particularly during low flow, when the relative influence of tides is large compared to river discharge. Although the data presented in this paper are not sufficient to predict how the Mekong changes between spring and neap tidal conditions, we expect the relative importance of the terms in the decomposition to vary throughout the fortnightly tidal cycle. For example, in the Tamar estuary, *Uncles et al.* [1986] found that tidal pumping (i.e., F_T) is more important during spring tides, and vertical shear—that is, F_E—dominates during neap tides.

The sign of F_T during low flow varied between the sections (Figure 12). The directionality of tidal pumping, one component of F_T, has been linked to channel depth in other mesotidal estuarine settings. In the York River estuary, the flux due to tidal pumping is downstream at the shoals and upstream in the deeps [*Scully and Friedrichs*, 2007]; although our decomposition considers each cross section as a whole, the mean depth at section A is shallower than at B or C, which is consistent with these findings. Given the limitations inherent to a single survey vessel, spatial and temporal variations of the system may be partially conflated in the observed data, which could also influence the variability in magnitude (and potentially direction) of the decomposed terms.

The residual flow, sediment flux, and inferred sediment-transport pathways during high and low flow (Figure 13) illustrate the complexities of transport dynamics in the transition between tidal river and estuary, and have similarities with previous work on the Mekong and other moderate-to-large river systems. On the Fraser River, Canada, *Milliman* [1980] observed that the majority of the sediment discharge occurred during the high-flow freshet. During low flow, there was little or no seaward transport of sediment, and near-bottom sediment transport was landward. Similarly, river discharge controls sediment transport to the ocean in the Changjiang River estuary, China [*Milliman et al.*, 1985]. Flux decomposition in the Hudson estuary revealed the importance of the advective river term to downstream sediment flux, particularly during the freshet [*Geyer et al.*, 2001]. This result highlights the variable strength of the estuarine circulation as a function of measurement location and timing within the tidal cycle.

Variability in sediment discharge over seasonal or longer time scales has been documented in other deltas with large freshwater reaches dominated by tidal processes. At inter-annual time scales on the Fly River delta, Papua New Guinea, estuarine processes extend past channel mouths during non-El Niño conditions, and sediment related to the estuarine turbidity maximum (ETM) can escape the mouth area. During El Niño, which corresponds to decreased river discharge, the ETM is trapped landward of the mouth, even during spring tides, which restricts seaward delivery of sediment [*Ogston et al*., 2008].

Conditions on the Mekong shelf are congruent with our findings of sediment export during high flow and import during low flow. In an earlier high-flow shelf study, river-derived SSC was observed 50–60 km offshore during the southwest summer monsoon [*Anikiyev et al*., 1986], and modeling studies show significant seasonality with fluvial sediment delivery and deposition near the mouth of the Mekong [*Xue et al*., 2012]. The findings of these studies are consistent with the river-dominated sediment export during high flow observed in the present study. Waves during the low-flow, winter-monsoon period likely resuspended previously deposited high-flow riverine sediment. A portion of this sediment may be transported toward the southwest [*Xue et al*., 2012], and estuarine processes enable additional transport of this sediment back into the distributary channels.

4.3.2. Extrapolated Sediment Discharge

Generating yearly sediment discharge estimates within tidal rivers is challenging but worth considering—even with a limited data set—because of a dearth of similar measurements on the Mekong and other large-tropical rivers worldwide. A number of assumptions must be made, including the temporal distribution of sediment flux over the year and flow partitioning among distributary channels. The discharge record at Can Tho (Figure 2) suggests an approximately equal temporal distribution of high-flow and low-flow conditions. Using this assumption and applying our Dinh An sediment-export values (1 t s^{-1} during high flow and −0.3 t s^{-1} during low flow) evenly across a year, the yearly Dinh An suspended-sediment discharge would be about 11 Mt yr^{-1}. Applying the flow partitioning of *Nguyen et al*. [2008] to this value results in 15 Mt yr^{-1} exported from the Song Hau distributary (i.e., Dinh An and Tran De channels), and about 40 Mt yr^{-1} from the Mekong River as a whole. In order to interpret this new estimate, we look to previous values from other studies, though they are based on scarce data often collected far from the mouth. Early estimates of 170–190 Mt yr^{-1} were made in the 1960s at stations 1000 km or more upstream of the mouth [*Economic Commission for Asia and the Far East*, 1966; *Holeman*, 1968]. A discharge of 178 Mt yr^{-1} was estimated 850 km from the mouth, with a notation that perhaps only 100–150 Mt yr^{-1} are delivered to the ocean [*Härden and Sundborg*, 1992], implying deposition of 26–44% of the sediment load in the downstream floodplain and delta. Sediment discharge has also been estimated on longer-time scales: *Ta et al*. [2002] computed an average discharge of 144 Mt yr^{-1} for the late Holocene, based on Mekong delta sediment-volume analysis. This type of approach may be more directly comparable to our results than upstream estimates, but the vast difference in time scales limits the utility of the comparison. One recent and generally accepted estimate is 110 Mt yr^{-1} today and 150 Mt yr^{-1} before damming and other impoundment [*Milliman and Farnsworth*, 2011], but this estimate again is based on a synthesis of gauged values far from the mouth and does not account for deposition in the tidal reach. Our sediment discharge value is 60–80% less than these estimates made upstream, and 60% less than one previous estimate at the mouth [*Härden and Sundborg*, 1992]. The difference between our value and previous estimates could suggest significant deposition on the floodplain and delta, seaward of prior upstream estimates, or a dramatically changing Mekong sediment-discharge rate; temporary sediment storage within the distributary channels themselves could also play a role. It could also indicate a distribution of sediment discharge among the distributary channels that is different from water discharge or one that varies with seasonal river flow.

To put the discharge implied by our measurements near the mouth further into the context of previous (upstream) estimates, we consider two alternative sediment-discharge scenarios. First, how would the yearly discharge magnitude change if there were zero net sediment import or export during low flow instead of the observed sediment import of −0.3 t s^{-1}? In this case, the yearly discharge would be controlled by the high-flow condition, which would be active for half the year, and the resultant yearly Mekong discharge would be about 60 Mt yr^{-1}. As above, this value is markedly smaller than previous estimates of sediment discharge.

Second, what conditions would be necessary to obtain sediment discharge at the mouth similar to the modern estimate of 110 Mt yr^{-1}? A scenario wherein the Dinh An channel operates as a high-flow system

throughout the year is required: in this situation, Dinh An sediment discharge would be about 32 Mt yr^{-1}, and, using the same scaling as above, total Mekong sediment discharge would be about 120 Mt yr^{-1}. This value, although a severe overestimate based on our observations, is comparable to modern estimates and yet is still considerably smaller than oft-cited values of 170 Mt yr^{-1} or more.

Our computed sediment discharge is seasonally limited and requires several large but necessary simplifying assumptions. It was, however, obtained closer to the mouth than any other existing estimate in the Mekong or in most other large, tidally influenced rivers worldwide. This discharge estimate provides a rare additional data point that reinforces the notion that the lowermost ungauged sections of large rivers are important traps of sediment. At a minimum, the insights gained from the estimate illustrate the dynamic variability of the tidal Mekong and its changing sedimentary role with seasonal discharge levels.

4.4. Geomorphic Response

In addition to modifying water-column characteristics, the seasonal pattern of suspended-sediment export during high flow and import during low flow alters the bed of the lower Mekong River. The coarser grain-size distributions in deep regions of the distributary channels during high flow are consistent with a system that mobilizes and transports fine particles to locations downstream, as observed in the residual flux, especially F_R (Figure 12). During high flow, shallow locations, especially at section B, exhibited finer bed sediment (Figure 7), resulting from the spatially heterogeneous flow dynamics and sediment resuspension. In contrast, the finer bed sediment at all locations during low flow is representative of a system that imports (via landward-directed F_R and F_T) and seasonally stores fine-grained sediment that is remobilized during subsequent high-flow periods.

The migration of the coarse region from within the Dinh An channel during high flow to above Cu Lao Dung during low flow suggests a shift in the location and behavior of fine-sediment trapping processes. During high flow, large bed stresses and a lack of salinity preclude the deposition of mud in the deep thalweg regions, and the presence of mud balls suggests flow scouring of the river bed. Even though ETM-like high SSC near the toe of the salt wedge was present during high flow near the river mouth (Figures 3 and 4), sediment trapping associated with the ETM was not evident in the bed-sediment characteristics of the distributary channels (Figure 7).

During low flow, which had maximum flow velocities similar to those during high flow, the increase in fine-grained sediment on the bed was likely due to flocculation and trapping processes related to the partially mixed estuarine regime that penetrated farther into the distributaries than during high flow. The general increase in SSC with distance upstream (Table 1) and colocation of the freshwater-saltwater interface suggest an ETM region at or just downstream of section C. ETMs often form at or near the head of salinity intrusion [*Dyer*, 1995], and section C during low flow captured the freshwater-saltwater interface. The fine-grained bed sediment at A and B suggests significant sediment trapping in those locations, but the mud cap imported during low flow did not extend past the upper limit of Cu Lao Dung. Indeed, the coarser grain size at the left and center stations of section C indicates that it was upstream of significant deposition related to estuarine trapping. The finer material at the right station of C, however, is intriguing. The right station had a lower mean salinity and reduced flood dominance compared to the left and center stations (Figure 5), which would generally discourage sediment trapping, even though fine sediment was prevalent on the bed there (Figure 7). A potential explanation can be found in the geomorphic setting of the right station at C, which is a direct upstream extension of the Tran De channel (Figure 1). Anecdotal evidence and historical aerial imagery suggest that Tran De is evolving to be a less important conduit for flow and sediment flux, and may in fact be a preferential location of sediment deposition. This evolution might explain why more fine bed sediment is present at the right station of section C, despite its lower salinity and reduced flood dominance.

Bedload dynamics are essential to fluvial [*Osterkamp*, 1998] and tidal [*Dalrymple et al*., 2003; *Harris et al*., 2004] landform generation and maintenance. Our observations suggest that the near-bed suspended-sediment pathways, which can be indicative of bedload-transport patterns, also support the development and maintenance of the rapidly prograding islands of the Mekong. At the upstream (closer to the left bank) island near section C, sediment deposition arising from the residual upstream flow (Figure 10) and sediment flux (Figure 11) may contribute to the island's progradation. Our data at section C are from only the low-flow period, but provide a glimpse into what is potentially an island-building flow regime, where sediment

import via estuarine circulation and tidal pumping seasonally nourishes the downstream ends of channel islands.

Farther downstream, at section A, the mid-channel bar resembles the linear subaqueous ridges that often form in river mouths of tide-dominated systems [*Wright*, 1977]. These ridges are thought to be generated by lateral convergence of sediment from ebb-dominated and flood-dominated channels. Indeed, during low flow, the right channel is more flood dominated with respect to velocity (Figures 5 and 10) than the left channel, and sediment is generally imported in the right channel and exported via the left channel (Figures 11 and 13). This pattern of sediment transport around the shoal may be related to the shoal's maintenance and, ultimately, its emergence as another channel island [*Hori et al*., 2002].

5. Conclusions

We have presented water-column and bed-sediment time-series observations made along the lowermost 30 km of the tidal Mekong River. These measurements include water level, flow velocity, salinity, SSC, and bed-sediment grain size, and they expand the present dynamical understanding of large-tropical deltas under varying seasonal discharge. Our conclusions are as follows:

1. The flow and sediment dynamics of the tidal Mekong River undergo a comprehensive regime change between high-seasonal and low-seasonal discharge. This change is highlighted by the transition from a tidal freshwater system with an ephemeral salt wedge to a partially mixed estuarine system.
2. The measured freshwater discharge was consistent with long-term discharge records during high flow but lower than average during low flow. The residual flow was downstream throughout the measured cross sections during high flow and spatially varying during low flow, signifying the importance of baroclinic forcing during periods of low freshwater input.
3. During high flow, Dinh An residual sediment discharge was seaward at a rate of about 1 t s^{-1}, and during low flow it was spatially variable and landward at a rate of 0.3 t s^{-1}. These rates scale to a yearly sediment discharge to the East Sea of 11 Mt yr^{-1} for the Dinh An channel and 40 Mt yr^{-1} for the entire Mekong River. This value is about 65% less than most previous estimates of Mekong sediment discharge. Although this discharge value was derived from a data set with limited temporal and spatial coverage, and thus has a relatively high degree of uncertainty, it remains valuable because it was derived for a location without previous estimates of this kind.
4. Decomposition of the sediment flux reveals that the river component was most important during high flow. Baroclinic and tidal processes, especially local resuspension, were more important during low flow.
5. Residual sediment flux was seaward throughout the water column during high flow. During low flow, residual sediment flux was landward in deep regions and seaward in the upper water column. These pathways provide evidence for larger-scale mutually evasive flow patterns (sediment import via Dinh An and export via Tran De) around Cu Lao Dung during low flow.
6. Seasonal flow dynamics are reflected in seabed grain-size characteristics, wherein grain size is variable to coarse during high flow and finer during low flow. The residual flow and sediment-flux patterns also support the maintenance and progradation of mid-channel islands.

Acknowledgments

We are grateful for the guidance, assistance, and friendship of Rich Nguyen. Thanks also to Rip Hale, Kevin Simans, Julia Marks, and the students and staff of Can Tho University, for field and laboratory assistance. This work was funded by the Office of Naval Research, award numbers N00014-12-1-0181, N00014-13-1-0127, and N00014-13-1-0781. DJN was partially supported by a National Defense Science and Engineering Graduate Fellowship. The data analyzed in this work are available upon request to the first author (nowacki@uw.edu).

References

Allen, G., J. Salomon, P. Bassoullet, Y. du Penhoat, and C. de Grandpre (1980), Effects of tides on mixing and suspended sediment transport in macrotidal estuaries, *Sediment. Geol.*, *26*, 69–90.

Anikiyev, V., O. Zaytsev, T. T. Hieu, I. Savil'yeva, Y. Starodubtsev, and Y. Shumilin (1986), Variation in the space-time distribution of suspended matter in the coastal zone of the Mekong River, *Oceanology*, *26*(6), 725–729.

Bale, A., A. Morris, and R. Howland (1985), Seasonal sediment movement in the Tamar Estuary, *Oceanol. Acta*, *8*(1), 1–6.

Barua, D. K. (1990), Suspended sediment movement in the estuary of the Ganges-Brahmaputra-Meghna river system, *Mar. Geol.*, *91*, 243–253.

Bell, H. S. (1940), Armored mud balls: Their origin, properties, and role in sedimentation, *J. Geol.*, *48*(1), 1–31.

Dalrymple, R. W., E. K. Baker, P. T. Harris, and M. G. Hughes (2003), Sedimentology and stratigraphy of a tide-dominated foreland-basin delta (Fly River, Papua New Guinea), in *Tropical Deltas of Southeast Asia—Sedimentology, Stratigraphy, and Petroleum Geology*, pp. 147–174, Soc. for Sediment. Geol., Tulsa, Okla.

Dronkers, J., and J. van de Kreeke (1986), Experimental determination of salt intrusion mechanisms in the Volkerak estuary, *Neth. J. Sea Res.*, *20*(1), 1–19, doi:10.1016/0077-7579(86)90056-6.

Dunne, T., L. Mertes, and R. Meade (1998), Exchanges of sediment between the flood plain and channel of the Amazon River in Brazil, *Geol. Soc. Am. Bull.*, *110*(4), 450–467, doi:10.1130/0016-7606(1998)110 < 0450:EOSBTF>2.3.CO;2.

Dyer, K. (1974), The salt balance in stratified estuaries, *Estuarine Coastal Mar. Sci.*, *2*(3), 273–281, doi:10.1016/0302-3524(74)90017-6.

Dyer, K. R. (1978), The balance of suspended sediment in the Gironde and Thames estuaries, in *Estuarine Transport Processes*, edited by B. Kjerfve, pp. 135–146, Univ. of South Carolina Press, Columbia, S. C.
Dyer, K. R. (1995), Sediment transport processes in estuaries, in *Geomorphology and Sedimentology of Estuaries*, edited by G. Perillo, pp. 423–449, Elsevier Sci., Amsterdam, Netherlands.
Dyer, K. R. (1997), *Estuaries: A Physical Introduction*, 2nd ed., 195 pp., John Wiley, Chichester, U. K.
Economic Commission for Asia and the Far East (1966), *A Compendium of Major International Rivers in the ECAFE Region*, U. N. Publ., N. Y.
Fischer, H. B. (1972), Mass transport mechanisms in partially stratified estuaries, *J. Fluid Mech.*, *53*, 671–687, doi:10.1017/S0022112072000412.
Fischer, H. B. (1976), Mixing and dispersion in estuaries, *Ann. Rev. Fluid Mech.*, *8*, 107–133, doi:10.1146/annurev.fl.08.010176.000543.
Fujii, H., H. Garsdal, P. Ward, M. Ishii, K. Morishita, and T. Boivin (2003), Hydrological roles of the Cambodian floodplain of the Mekong River, *Int. J. River Basin Manage.*, *1*(3), 1–14, doi:10.1080/15715124.2003.9635211.
Gagliano, S. M., and W. McIntire (1968), Reports on the Mekong River Delta, technical report 57, Coastal Stud. Inst., Louisiana State Univ.
Gelfenbaum, G. (1983), Suspended-sediment response to semidiurnal and fortnightly tidal variations in a mesotidal estuary: Columbia River, U.S.A., *Mar. Geol.*, *52*(1–2), 39–57, doi:10.1016/0025-3227(83)90020-8.
Geyer, W. R., J. D. Woodruff, and P. Traykovski (2001), Sediment transport and trapping in the Hudson River estuary, *Estuaries*, *24*(5), 670–679.
Giddings, S. N., S. G. Monismith, D. A. Fong, and M. T. Stacey (2013), Using depth-normalized coordinates to examine mass transport residual circulation in estuaries with large tidal amplitude relative to the mean depth, *J. Phys. Oceanogr.*, *44*, 128–148, doi:10.1175/JPO-D-12-0201.1.
Goodbred, S. L., and S. A. Kuehl (1998), Floodplain processes in the Bengal Basin and the storage of Ganges-Brahmaputra river sediment: An accretion study using ^{137}Cs and ^{210}Pb geochronology, *Sediment. Geol.*, *121*, 239–258.
Hansen, D. V., and M. Rattray, Jr. (1966), New dimensions in estuary classification, *Limnol. Oceanogr.*, *11*(3), 319–326.
Härden, P., and A. Sundborg (1992), The lower Mekong basin suspended sediment transport and sedimentation problems, technical report, Mekong Secr., Uppsala.
Harris, P. T. (1988), Large-scale bedforms as indicators of mutually evasive sand transport and the sequential infilling of wide-mouthed estuaries, *Sediment. Geol.*, *57*(1988), 273–298.
Harris, P. T., M. G. Hughes, E. K. Baker, R. W. Dalrymple, and J. B. Keene (2004), Sediment transport in distributary channels and its export to the pro-deltaic environment in a tidally dominated delta: Fly River, Papua New Guinea, *Cont. Shelf Res.*, *24*(19), 2431–2454, doi:10.1016/j.csr.2004.07.017.
Holeman, J. N. (1968), The sediment yield of major rivers of the world, *Water Resour. Res.*, *4*(4), 737–747, doi:10.1029/WR004i004p00737.
Hori, K., Y. Saito, Q. Zhao, and P. Wang (2002), Architecture and evolution of the tide-dominated Changjiang (Yangtze) River delta, China, *Sediment. Geol.*, *146*(3–4), 249–264, doi:10.1016/S0037-0738(01)00122-1.
Hu, J., H. Kawamura, H. Hong, and Y. Qi (2000), A review on the currents in the South China Sea: Seasonal circulation, South China Sea warm current and Kuroshio intrusion, *J. Oceanogr.*, *56*, 607–624.
Hughes, F., and M. Rattray, Jr. (1980), Salt flux and mixing in the Columbia River Estuary, *Estuarine Coastal Mar. Sci.*, *10*, 479–493.
Kineke, G., and R. Sternberg (1995), Distribution of fluid muds on the Amazon continental shelf, *Mar. Geol.*, *125*, 193–233, doi:10.1016/0025-3227(95)00013-O.
Kuehl, S. A., C. A. Nittrouer, M. A. Allison, L. E. C. Faria, D. A. Dukat, J. M. Jaeger, T. D. Pacioni, A. G. Figueiredo, and E. C. Underkoffler (1996), Sediment deposition, accumulation, and seabed dynamics in an energetic fine-grained coastal environment, *Cont. Shelf Res.*, *16*(516), 787–815, doi:10.1016/0278-4343(95)00047-X.
Kummu, M., and O. Varis (2007), Sediment-related impacts due to upstream reservoir trapping, the Lower Mekong River, *Geomorphology*, *85*(3–4), 275–293, doi:10.1016/j.geomorph.2006.03.024.
Lerczak, J. A., W. R. Geyer, and R. J. Chant (2006), Mechanisms driving the time-dependent salt flux in a partially stratified estuary, *J. Phys. Oceanogr.*, *36*, 2296–2311.
Lu, X. X., and R. Y. Siew (2006), Water discharge and sediment flux changes over the past decades in the Lower Mekong River: Possible impacts of the Chinese dams, *Hydrol. Earth Syst. Sci.*, *10*(2), 181–195, doi:10.5194/hess-10-181-2006.
MacCready, P., and N. Banas (2011), Residual circulation, mixing, and dispersion, in *Treatise on Estuarine and Coastal Science*, edited by E. Wolanski and D. McLusky, pp. 75–89, Academic Press, London, U. K.
Meade, R. H. (1969), Landward transport of bottom sediments in estuaries of the Atlantic coastal plain, *J. Sediment. Petrol.*, *39*(1), 222–234.
Mekong River Commission (2009), The Flow of the Mekong, technical report, Mekong River Comm, MRC Management Information booklet series No. 2.
Mekong River Commission (2014), Data Portal.
Mertes, L. A. K., T. Dunne, and L. A. Martinelli (1996), Channel-floodplain geomorphology along the Solimões-Amazon River, Brazil, *Geol. Soc. Am. Bull.*, *108*(9), 1089–1107, doi:10.1130/0016-7606(1996)108 < 1089:CFGATS>2.3.CO;2.
Milliman, J. D. (1980), Sedimentation in the Fraser River and its estuary, southwestern British Columbia (Canada), *Estuarine Coastal Mar. Sci.*, *10*, 609–633.
Milliman, J. D., and K. L. Farnsworth (2011), *River Discharge to the Coastal Ocean: A Global Synthesis*, 392 pp., Cambridge Univ. Press, Cambridge, U. K.
Milliman, J. D., S. Huang-Ting, Y. Zuo-Sheng, and R. H. Meade (1985), Transport and deposition of river sediment in the Changjiang estuary and adjacent continental shelf, *Cont. Shelf Res.*, *4*(1/2), 37–45.
Nguyen, A. D., H. H. Savenije, D. N. Pham, and D. T. Tang (2008), Using salt intrusion measurements to determine the freshwater discharge distribution over the branches of a multi-channel estuary: The Mekong Delta case, *Estuarine Coastal Shelf Sci.*, *77*(3), 433–445, doi:10.1016/j.ecss.2007.10.010.
Nguyen, T., and H. Tanaka (2007), Study on the effect of morphology change on salinity distribution in the Dinh An estuary, lower Mekong River of Vietnam, *J. Coastal Res.*, *SI 50*, 268–272.
Nittrouer, C. A., S. A. Kuehl, R. W. Sternberg, A. G. Figueiredo, and L. E. C. Faria (1995), An introduction to the geological significance of sediment transport and accumulation on the Amazon continental shelf, *Mar. Geol.*, *125*, 177–192.
Ogston, A. S., R. W. Sternberg, C. A. Nittrouer, D. P. Martin, M. A. Goñi, and J. S. Crockett (2008), Sediment delivery from the Fly River tidally dominated delta to the nearshore marine environment and the impact of El Niño, *J. Geophys. Res.*, *113*, F01S11, doi:10.1029/2006JF000669.
Osterkamp, W. (1998), Processes of fluvial island formation, with examples from Plum Creek, Colorado and Snake River, Idaho, *Wetlands*, *18*(4), 530–545, doi:10.1007/BF03161670.

Postma, H. (1967), Sediment transport and sedimentation in the estuarine environment, in *Estuaries*, edited by G. H. Lauff, pp. 158–179, Am. Assoc. for the Adv. of Sci., Washington, D. C.
Ralston, D. K., W. R. Geyer, J. a. Lerczak, and M. Scully (2010), Turbulent mixing in a strongly forced salt wedge estuary, *J. Geophys. Res.*, *115*, C12024, doi:10.1029/2009JC006061.
Ralston, D. K., W. R. Geyer, and J. C. Warner (2012), Bathymetric controls on sediment transport in the Hudson River estuary: Lateral asymmetry and frontal trapping, *J. Geophys. Res.*, *117*, C10013, doi:10.1029/2012JC008124.
Savenije, H. H. (2005), *Salinity and Tides in Alluvial Estuaries*, Elsevier, Amsterdam.
Schubel, J. (1968), Turbidity maximum of the northern Chesapeake Bay, *Science*, *161*(3845), 1013–1015.
Scully, M. E., and C. T. Friedrichs (2007), Sediment pumping by tidal asymmetry in a partially mixed estuary, *J. Geophys. Res.*, *112*, C07028, doi:10.1029/2006JC003784.
Su, J., and K. Wang (1986), The suspended sediment balance in Changjiang estuary, *Estuarine Coastal Shelf Sci.*, *23*, 81–98.
Syvitski, J. P. M., and A. Kettner (2011), Sediment flux and the Anthropocene, *Philos. Trans. R. Soc. A*, *369*(1938), 957–975, doi:10.1098/rsta.2010.0329.
Ta, T. K. O., V. L. Nguyen, M. Tateishi, I. Kobayashi, S. Tanabe, and Y. Saito (2002), Holocene delta evolution and sediment discharge of the Mekong River, southern Vietnam, *Quat. Sci. Rev.*, *21*, 1807–1819.
Ta, T. K. O., V. L. Nguyen, M. Tateishi, I. Kobayashi, and Y. Saito (2005), Holocene delta evolution and deposition models of the Mekong River Delta, southern Vietnam, in *River Deltas—Concepts, Models, and Examples*, edited by L. Giosan and J. P. Bhattacharya, pp. 453–466, Soc. for Sediment. Geol., Tulsa, Okla.
Uncles, R., and M. Jordan (1979), Residual fluxes of water and salt at two stations in the Severn Estuary, *Estuarine Coastal Mar. Sci.*, *9*(3), 287–302, doi:10.1016/0302-3524(79)90042-2.
Uncles, R., R. Elliott, and S. Weston (1985a), Dispersion of salt and suspended sediment in a partly mixed estuary, *Estuaries*, *8*(3), 256–269.
Uncles, R., R. Elliott, and S. Weston (1985b), Observed fluxes of water, salt and suspended sediment in a partly mixed estuary, *Estuarine Coastal Shelf Sci.*, *20*(2), 147–167, doi:10.1016/0272-7714(85)90035-6.
Uncles, R. J., R. C. A. Elliott, and S. A. Weston (1986), Synoptic observations of salinity, suspended sediment and vertical current structure in a partly mixed estuary, in *Physics of Shallow Estuaries and Bays*, vol.16, edited by C. van de Kreeke, pp. 58–70, Springer, Berlin.
Unverricht, D., W. Szczuciński, K. Stattegger, R. Jagodziński, X. T. Le, and L. L. W. Kwong (2013), Modern sedimentation and morphology of the subaqueous Mekong Delta, Southern Vietnam, *Global Planet. Change*, *110*, 223–235, doi:10.1016/j.gloplacha.2012.12.009.
Walters, R., R. Cheng, and T. Conomos (1985), Time scales of circulation and mixing processes of San Francisco Bay waters, *Hydrobiologia*, *129*, 13–36.
Wolanski, E., N. Ngoc Huan, L. Trong Dao, N. Huu Nhan, and N. Ngoc Thuy (1996), Fine-sediment dynamics in the Mekong River estuary, Vietnam, *Estuarine Coastal Shelf Sci.*, *43*(5), 565–582.
Wolanski, E., N. Nhan, and S. Spagnol (1998), Sediment dynamics during low flow conditions in the Mekong River Estuary, Vietnam, *J. Coastal Res.*, *14*(2), 472–482.
Woodruff, J. D., W. R. Geyer, C. K. Sommerfield, and N. W. Driscoll (2001), Seasonal variation of sediment deposition in the Hudson River estuary, *Mar. Geol.*, *179*, 105–119.
Wright, L. (1977), Sediment transport and deposition at river mouths: A synthesis, *Bull. Geol. Soc. Am.*, *88*(6), 857, doi:10.1130/0016-7606(1977)88 < 857:STADAR>2.0.CO;2.
Wright, L. (1985), River Deltas, in *Coastal Sedimentary Environments*, edited by R. A. Davis, pp. 1–76, Springer, New York.
Xue, Z., J. P. Liu, D. DeMaster, L. Van Nguyen, and T. K. O. Ta (2010), Late Holocene evolution of the Mekong subaqueous delta, southern Vietnam, *Mar. Geol.*, *269*(1–2), 46–60, doi:10.1016/j.margeo.2009.12.005.
Xue, Z., J. P. Liu, and Q. Ge (2011), Changes in hydrology and sediment delivery of the Mekong River in the last 50 years: Connection to damming, monsoon, and ENSO, *Earth Surf. Processes Landforms*, *36*(3), 296–308, doi:10.1002/esp.2036.
Xue, Z., R. He, J. Liu, and J. C. Warner (2012), Modeling transport and deposition of the Mekong River sediment, *Cont. Shelf Res.*, *37*, 66–78, doi:10.1016/j.csr.2012.02.010.

Erratum

In the originally published version of this article, the affiliation for the corresponding author was incomplete. The affiliation has since been corrected, and this version may be considered the authoritative version of record.